



**HAL**  
open science

## Design of Biocompatible Multifunctional Hydrogels with Stearyl Methacrylate and Vinylpyrrolidone

Hüsna Kılıç, Deniz Ceylan Tuncaboylu, Aslıhan Argun, Dilek Öztürk Civelek

► **To cite this version:**

Hüsna Kılıç, Deniz Ceylan Tuncaboylu, Aslıhan Argun, Dilek Öztürk Civelek. Design of Biocompatible Multifunctional Hydrogels with Stearyl Methacrylate and Vinylpyrrolidone. ACS Applied Polymer Materials, 2022, 4 (3), pp.1717 - 1727. 10.1021/acsapm.1c01565 . hal-04608526

**HAL Id: hal-04608526**

**<https://hal.science/hal-04608526>**

Submitted on 11 Jun 2024

**HAL** is a multi-disciplinary open access archive for the deposit and dissemination of scientific research documents, whether they are published or not. The documents may come from teaching and research institutions in France or abroad, or from public or private research centers.

L'archive ouverte pluridisciplinaire **HAL**, est destinée au dépôt et à la diffusion de documents scientifiques de niveau recherche, publiés ou non, émanant des établissements d'enseignement et de recherche français ou étrangers, des laboratoires publics ou privés.



Distributed under a Creative Commons Attribution 4.0 International License

# Design of Biocompatible Multifunctional Hydrogels with Stearyl Methacrylate and Vinylpyrrolidone

Hüsna Kılıç, Deniz Ceylan Tuncaboşlu,\* Aslıhan Argun, and Dilek Öztürk Civelek

Cite This: *ACS Appl. Polym. Mater.* 2022, 4, 1717–1727

Read Online

ACCESS |



Metrics &amp; More



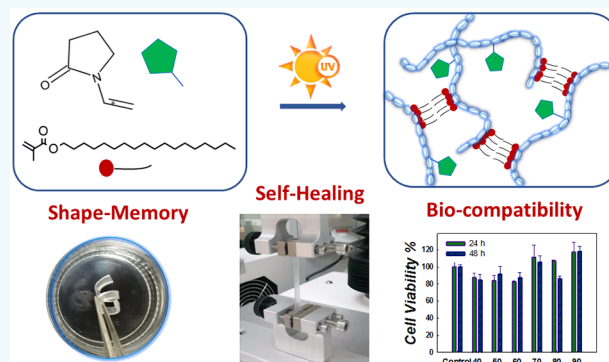
Article Recommendations



Supporting Information

**ABSTRACT:** Biofunctionality and biocompatibility are essential when tissue or organs are supplemented or replaced with a polymer based material. Here, we prepared stearyl methacrylate (SM) and vinylpyrrolidone (VP) based biocompatible SM-*x* networks with self-healing and shape memory properties. The mole ratios were gradually changed from hydrophilic to hydrophobic units between 10 and 90% to obtain gels meeting the requirements in various potential bioapplications. In addition to having a time-dependent viscoelastic character, the mechanical properties of the gels can be controlled by the amount of SM introduced into the reaction medium. Low SM content gels cannot fully return to their initial modulus values, while the gels formed with concentrations  $\geq 60\%$  are completely reversible due to the dynamic hydrophobic interactions, which is also effective in the self-healing behavior. Moreover, all of the networks can completely recall their permanent shape in seconds. The viability of human skin fibroblast cells, seeded on SM-*x* hydrogels, closely related to the water contact angle of the structures, was found to be over 82% at all *x* values. In the light of the findings, the wide range of properties of SM-*x* gel samples may show significant potential to address needs in a variety of biomedical applications.

**KEYWORDS:** self-healing, shape memory, stearyl methacrylate, vinylpyrrolidone, biocompatibility



## 1. INTRODUCTION

Hydrogels are three-dimensional cross-linked polymer networks, which can absorb and retain a large amount of water. Polymeric networks have recently evolved from classical structures to “smart” materials, also known as new generation hydrogels, which alter their physical and chemical properties with various stimuli such as pH, temperature, chemical structures, electric field, or light. Tunable properties and functionalities, chemical and physical diversity, as well as the simple preparation methods, combined with stimuli responsiveness, make smart gels ideal candidates for applications in a variety of fields from tissue engineering to medicine and soft robotics.

When functions of tissues or organs are substituted by a polymer based device, biofunctionality is required. Self-healing ability is one of the superior properties of natural materials that extend the life of living organisms. Self-healing polymers (SHPs) can repair mechanical damage autonomously or in the presence of a stimuli. Even though synthetic hydrogels are very similar to biological tissues, they do not possess inherent healing ability mainly because of their rigid building blocks that cannot migrate across the damage or dissipate the crack energy. It has been used as an inspiration for the development of smart materials by imitating the extraordinary properties of biological systems. Research on self-healing hydrogels has been started just 20 years

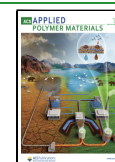
ago accompanied by a stepwise increase in the number of scientific publications. The main strategies to obtain a gel with self-healing ability depend on creating reversible cross-links with infinite lifetimes inside the network structure, such as hydrophobic interactions,<sup>1–10</sup> dynamic ester bonds,<sup>11–13</sup> complexation,<sup>14,15</sup> and host–guest interactions.<sup>16–18</sup>

Having the growing interest in self-healing materials in mind, shape memory polymers (SMPs) have the ability to recover the permanent shape from a temporary one in a predefined way on demand when exposed to a stimulus. Typically, shape memory hydrogels provide a polymer network architecture consisting of a hybrid-cross-linked network structure composed of net-points and switching segments as permanent and temporary cross-links, respectively. While the net-points determine the permanent shape of the hydrogel which are interconnected by the chain segments, the physical cross-links formed by solidification of the switching segments below the melting or glass transition temperatures fix the temporary shape.<sup>19</sup> At

**Received:** November 9, 2021

**Accepted:** February 10, 2022

**Published:** February 22, 2022



present, most investigated SMPs are thermosensitive, which means that the SME is triggered by heat.<sup>20</sup> SMPs also have great potential in many application areas such as biocompatible actuators and implant devices for minimally invasive surgery in the medical field.

Today, the design of advanced materials with improved features and capability of performing complex functions such as self-healing and shape memory is supported. To prepare hydrogels with both self-healing and shape memory properties, there must be strong physical cross-links that act as net-points within the structure and weak physical cross-links for switching. In the literature, there are studies on hydrogels with both self-healing and shape memory properties.<sup>21</sup> Recently, a simple method was shown that bulk photopolymerization of hydrophilic and hydrophobic monomers generates self-healing hydrogels with a shape memory effect due to the presence of hydrophobic associations and crystalline domains acting as the net-points and switching segments, respectively.<sup>22</sup> The reported gels were designed up to 50% of the hydrophobic monomer content in the total monomer feed, and no biocompatibility studies have been performed.<sup>23,24</sup>

Within the scope of this study, high mechanical strength semicrystalline hydrogels with heat-responsive self-healing and shape memory functions were synthesized and characterized. Smart gels were prepared by the bulk polymerization method using stearyl methacrylate (SM) and vinylpyrrolidone (VP) monomers in a wide range of hydrophobic monomer contents from 10 to 90%. While the presence of long hydrophobic chains provides gels with the ability to self-heal, the structure containing high amounts of crystalline regions allows the occurrence of the shape memory effect. In order to meet the requirements and standards in various potential bioapplications, the effects of hydrophilic and hydrophobic components in SM-*x* gels synthesized for the first time in the literature were investigated from the various aspects, including physical (e.g., swelling ratio, etc.), chemical (e.g., chemical composition, etc.), mechanical (e.g., tensile/compressive strength, Young's modulus, toughness, etc.), rheological (e.g., loss/storage modulus, etc.), and biological (e.g., biocompatibility, etc.) properties.

## 2. MATERIALS AND METHODS

**2.1. Materials.** 1-Vinyl-2-pyrrolidone 99% (VP), stearyl methacrylate (SM), a mixture of 65% *n*-octadecyl methacrylate and 35% *n*-hexadecyl methacrylate, and 2-hydroxy-40-(2-hydroxyethoxy)-2-methylpropiophenone (Irgacure 2959) were all purchased from Sigma-Aldrich and used without purification. Distilled water was used throughout this study. DMEM/F12 medium, fetal bovine serum, penicillin/streptomycin, and trypsin were purchased from Gibco (Thermo Fisher Scientific, US).

**2.2. Preparation of Hydrogels.** Hydrophilic monomer 1-vinyl-2-pyrrolidone (VP) and hydrophobic monomer stearyl methacrylate (SM) were used in hydrogel synthesis. Bulk polymerization of the SM and VP in the presence of Irgacure as an initiator was carried out for 24 h in a photoreactor (Kerman brand equipped with 18 Philips 8 W lamps and 15 Philips 6 W lamps emitting nominally at  $\lambda = 350$  nm). For the gel synthesis, the reaction solutions taken into plastic templates fixed with sealing tape and plastic pipettes were kept under UV light. SM/VP ratios were gradually changed to examine the effect of hydrophobic and hydrophilic components on the properties of the final gels. The hydrogels denoted by SM-*x* were prepared at a SM/VP molar ratio of  $x/100 - x$ . For monitoring the gel fractions, the gels were kept in distilled water until they reached swelling equilibrium after UV irradiation and their water was changed frequently (at least once a day). The gels that came to the swelling equilibrium were dried in a freeze-dryer. Gel

fractions were calculated by considering the weight ratio of the insoluble polymer remaining in the network to the initial sample.

**2.3. Characterization of Hydrogels. Swelling Measurements.** The SM-*x* networks synthesized in the photoreactor were cut in certain sizes, considering the tests to be carried out, and then, they were immersed into the water after recording the weights of the gels. Water was changed every day to remove unreacted components. Swelling kinetics and relative and equilibrium swelling values were determined at 50 °C by weight monitoring until the swelling balance was reached. Swelling measurements were performed in triplicate, with uncertainty indicating the standard deviation of measurement data. The swelling ratio of the hydrogels concerning the preparation state was determined gravimetrically by the equation  $m_{rel} = m_t/m_0$ , where  $m_t$  and  $m_0$  are the masses of the hydrogels after preparation and swollen states, respectively.

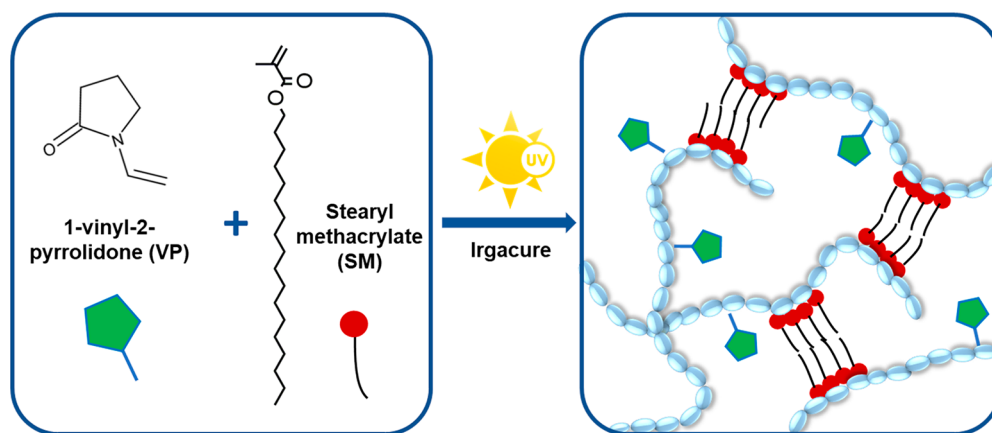
**Rheological Measurements.** SM-*x* gels with different monomer ratios were synthesized in the photoreactor. Besides, thanks to the photo unit (equipped with a Omnicure lamp, 365 nm), the gels were synthesized between plates of the rheometer, so the gelation kinetics were monitored in situ. Oscillatory measurements were performed between the parallel plates of a controlled shear rheometer (Physica MCR 102 Anton Paar, Germany). The upper plate (diameter 15 mm) was set at 0.5 mm before the onset of the reactions. During the rheological measurements, a solvent trap was used to minimize the evaporation. Time, frequency, and strain sweep measurements were used for the basic rheological characterization of the networks. Initially, the strain sweep was performed at a constant frequency of 1 Hz over the strain range 1–100% to determine the linear viscoelastic region (LVER) of the samples. The time sweep was measured at 24 °C at a frequency of  $f = 1$  Hz and a deformation amplitude of  $\gamma_0 = 0.1$  to ensure that the oscillatory deformation is within the LVER. The frequency sweep was conducted at 0.1% strain over the frequency range 0.1–100 Hz. The storage modulus ( $G'$ ) and loss modulus ( $G''$ ) and  $\tan \delta$  were used to evaluate the rheological properties of the gel samples. Two duplicate runs were done for each measurement to control the reproducibility of the system.

**Compression and Elongation Measurements.** Uniaxial compression and elongation tests of the cylindrical gel samples were conducted using a TA.XTplus Texture Analyzer with a 5 N load cell (Stable Micro Systems, Surrey, U.K.). Compression tests were carried out at a rate of 1 mm/min by utilizing the cylindrical probes of 5 mm in height. For reproducibility, at least seven samples were measured for each concentration and the results were averaged. Exponent software was used with the texture analyzer to record and analyze the results. The variables and parameters were calculated by macros written in the same software. The Young's modulus from the compression tests was calculated from the slope of stress–strain curves between the deformation of 5 and 15% which corresponds to the linear region.

**Differential Scanning Calorimetry (DSC) Analysis.** DSC measurements were conducted on a TA Instruments Discovery DSC 250 with a heating/cooling rate of 10 °C min<sup>-1</sup> under a nitrogen atmosphere. Approximately 5 mg of gel samples were sealed in aluminum pans for the scan between 0 and 200 °C. From the DSC curves, enthalpy changes during melting,  $\Delta H_m$ , were calculated from the peak areas. The degree of crystallinity,  $f$  %, that is, the fraction of polymer units in crystalline domains, was estimated by  $f_{cry} = x_{HM} \Delta H_m / \Delta H_M^\circ$ , where  $x_{HM}$  is the mole fraction of the hydrophobic monomer in the comonomer feed and  $\Delta H_M^\circ$  is the melting enthalpy of crystalline SM units.  $\Delta H_M^\circ$  was taken as 71.2 kJ mol<sup>-1</sup> from previous works on the melting behavior of long *n*-alkyl chains exhibiting a hexagonal crystal structure.<sup>25–27</sup>

**X-ray Measurements.** Wide-angle X-ray powder diffraction profiles were collected at room temperature, with a Bruker diffractometer (D2 Phaser, Bruker AXS GmbH) using Cu K $\alpha$  radiation ( $\lambda = 1.5406$  Å) and scans at a  $2\theta$  range of 5–90° with 0.02 steps at 30 kV and 10 mA. The crystallite size of alkyl units was calculated by XRD data by the Debye–Scherrer formula<sup>23</sup>

$$D = K\gamma/B \cos \theta \quad (1)$$

Scheme 1. Schematic Illustration of the Synthesis of the SM-*x* Networks in the Presence of Irgacure as a Photoinitiator

where  $K$  ( $K = 0.89$ ) is the Scherrer constant and  $B$  is the half peak width of the XRD peak of the measured sample;  $D$  is the average thickness of the sample grain in the direction of the crystal plane (nm); and  $\theta$  is the diffraction angle of the XRD peak. The parameter  $\gamma$  ( $\gamma = 0.154056$ ) is the wavelength of X-rays.

**Shape Memory Tests.** The shape memory properties of the hydrogels were quantified by a bending test in which the gel samples were initially heated in hot water.<sup>28</sup> After softening, the samples were folded in half and then cooled down to 5 °C to fix the temporary shape. Subsequently, the samples in a water bath were stepwise heated from 5 to 60 °C. In the last step, the transition from the temporary to the permanent shape was photographed to determine the corresponding equilibrium angle  $\theta_T$  at each temperature. Besides recording the time to recover the shape, the shape recovery ratio,  $R$ , was also calculated as follows:  $R = (\theta_T/180)$ .

**2.4. Biocompatibility Studies.** Human skin fibroblast cells CCD-986Sk (ATCC CRL-1947) were used in biocompatibility tests. Cells were cultured in DMEM/F12 (Gibco) medium containing 10% fetal bovine serum (FBS) and 1% penicillin/streptomycin. CCD cells were cultured, passaged, and stored according to the protocols advised by the brand. The desired numbers of cells were then seeded in the plates. The cytotoxicity of the gels was evaluated by using the direct contact test. Before biocompatibility studies, SM-*x* gels were kept in PBS solution containing 1% penicillin/streptomycin for 1 week. Additionally, they were UV sterilized before the experiment.

**Direct Contact Test.** The direct contact test was carried out according to ISO 10993-5:2009.<sup>29,30</sup> CCD cells ( $1 \times 10^5$  cells/well) were cultured in 24-well plates under the same condition; then, the medium in the seeded wells was discarded. SM-*x* networks were placed directly on the adhered cells, and fresh medium was added. They were incubated for 24 and 48 h in an incubator under 5% CO<sub>2</sub> at 37 °C. Three replicates were run for each gel sample, and control wells without any gel were left.

After the incubation period, viability of CCD cells was detected via MTT assay. In this assay, yellow 3-(4,5-dimethylthiazolyl-2)-2,5-diphenyltetrazolium bromide (MTT, Sigma, USA) was reduced by metabolically active cells. Gels were removed, and fresh medium containing MTT reagent (final concentration 0.5 mg/mL) was added to the plates; they were then incubated at 37 °C for 4 h. At the end of the application period, 250  $\mu$ L of dimethyl sulfoxide (DMSO, Sigma, USA) solution was added to dissolve the precipitated formazan crystals after removing the reagent from the wells.<sup>30</sup> To assess the cell metabolism, the absorbance/optical density (OD) was measured at 570 nm by using a microplate reader (BioTek Synergy H1, USA). Recorded OD results were evaluated according to the following equation:

$$\text{Percent cell viability} = \frac{\text{OD of experimental group}}{\text{OD of control group}} \times 100 \quad (2)$$

**Cell Adhesion Test.** After sterilization, SM-VP networks were placed on a 24-well plate in triplicate. Following the counting, the cells were seeded onto placed gels at a density of  $1 \times 10^5$  cells per gel in 50  $\mu$ L of culture medium and were left for 1 h before covering the gels with culture medium. Cells were left to grow on gels in the incubator at 37 °C under 5% CO<sub>2</sub> for 24 or 48 h. After this period, plates were washed with PBS to remove unattached cells and the cells were stained with 1  $\mu$ g/mL Hoechst dye and observed by using a fluorescence microscope (Zeiss Axio Observer Z1).

### 3. RESULTS AND DISCUSSION

In this paper, mechanically strong smart hydrogels with shape memory and self-healing functions have been designed and characterized. Free radical bulk polymerization of hydrophobic monomer stearyl methacrylate (SM) and hydrophilic monomer vinylpyrrolidone (VP) was performed by using Irgacure 2959 as the photoinitiator at a concentration of 0.1 w/v %. Mole ratios of the monomers were gradually changed from hydrophilic to hydrophobic ones between 10 and 90% to examine the effect of components on the properties of the final gels. Samples with the codes of SM-10, SM-20, and SM-30 were not used throughout the study due to the phase separation during the synthesis, as shown in Figure S1A. Considering the reactivity ratios of SM and VP with  $r_1 = 0.810$  and  $r_2 = 0.097$ , respectively, it means that SM is more reactive in the reaction compared to VP; thus, there is a kinetic preference for incorporation of SM into the copolymer structure.<sup>31–33</sup> As illustrated in Scheme 1, hydrophobic monomer SM with long side alkyl chains forms crystalline domains and/or hydrophobic associations in the presence of the bulky pyrrolidone units involving dipole–dipole interactions and leads to the formation of SM-*x* networks.

Before performing the gel syntheses in the photoreactor, reactions were monitored *in situ* with a rheometer under 365 nm UV light (Figure S1B). After 7 h of UV irradiation,  $G'$  was found to be higher than  $G''$ , which is the minimum time required for gelation to begin. Similar results were obtained at other concentrations, and it was decided to carry out the reactions in a photoreactor (Figure S1C). After 24 h of reaction in the reactor, SM-*x* networks were removed from the plastic pipettes and immersed into the water at 50 °C to reach their swelling equilibrium. While the surrounding water of the gels was replaced at certain intervals, weight changes were followed to monitor the swelling kinetics of the networks. As plotted in Figure S2, the decrease of the swelling equilibrium values gradually parallel to the  $x$  values up to 60 indicates that the long alkyl chains of SM molecules are effectively incorporated into

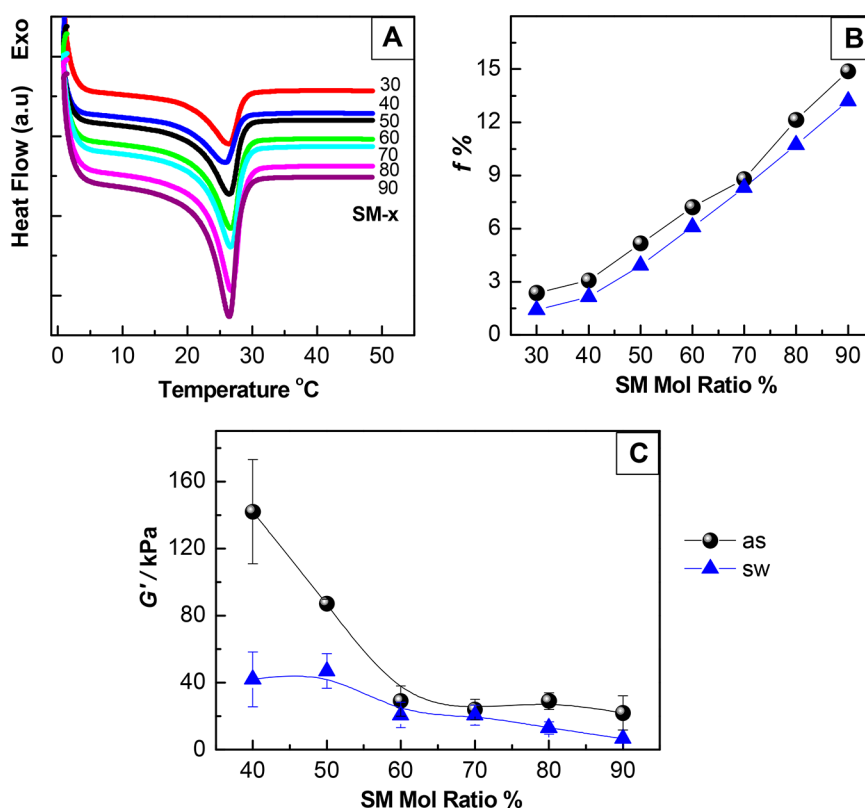


**Figure 1.** (A) DSC plots of the gels with various SM contents. (B) Crystallization fraction and (C) storage modulus  $G'$  of SM- $x$  networks as a function of SM mol ratio % as-prepared (black ●) and swollen states (blue ▲) at 37 °C.

the structure as cross-linkers. When the swelling kinetics depending on the  $x$  value is examined, a maximum is observed on the fourth day of the measurements. As with silk fibroin gels, where  $\beta$  sheet ( $\beta$ -sheet) structures act as cross-links, the gels shrink after swelling. This is a result of increased crystallinity due to increased stress from swelling.<sup>34</sup> While excessive swelling is observed at low  $x$  values where VP is high, the shrinkage due to the crystal structures formed by the rearrangement of long alkyl chains is much more pronounced. It shrinks in parallel with the decrease of the maximum VP in swelling kinetics.

The gel fraction ( $W_g$ ) values of 1 and above with decreasing water content in proportion to the increasing amount of hydrophobes indicate that all monomers in the feed are included in the SM- $x$  networks (Figure S3). Since the gels do not dry well at low SM ratios, the  $W_g$  slightly above 1 may be due to the increased hydrogen bonding at these concentrations. After reaching equilibrium, hydrogels were subjected to a series of characterization processes as-prepared and in the equilibrium swollen states. Initially, thermal properties of the networks were scanned by using DSC thermograms. As plotted in Figure S4, melting temperatures ( $T_m$ ) and crystallization temperatures ( $T_{cry}$ ) after synthesis and in the swollen states were identified through DSC analysis. Variations of the melting peaks as a function of SM feed content collected in Figure 1A and peak enthalpies of the thermograms were used to calculate the degree of crystallinity,  $f\%$ , originated from the side alkyl chains of SM. According to the  $f\%$ –SM mol ratio graph, crystallinity increases parallel to the amount of SM after synthesis and swollen states (Figure 1B).<sup>22</sup> Independent of the SM content, a slight decrease was observed in the  $f\%$  values by the swelling of the matrix.

To observe the viscoelastic nature of the gel and the gel strength in a shearing action, rheological characterization of the

network is indispensable. Therefore, after 1 day of reaction in the photoreactor, disk-shaped samples approximately 1 mm in thickness were subjected to the oscillatory measurements of time, frequency, and amplitude sweep. Considering the DSC data of the SM- $x$  networks, which are planned to be used in bio applications in the future, rheological measurements were carried out at 37 °C, a temperature above the  $T_m$  value of the gels. The storage moduli,  $G'$ , of the gels were plotted as a function of SM feed amounts in Figure 1C.  $G'$  values decrease rapidly due to increased SM concentrations up to a mol ratio of 60% but do not change much after this concentration. Since the measurements were made at 37 °C, that is, above the  $T_m$  value, the crystalline regions were melted. Therefore, the main factor determining the modulus values can be interpreted as the decrease in the amount of VP in the structure with increasing SM, which in turn reduces the dipole–dipole interactions in the cross-link density. When the same measurements were applied to the gels that reached the swelling equilibrium, it was observed that the  $G'$  decreased with a slight slope due to the increasing amount of SM. Another remarkable point in the figure is that the  $G'$  values of swollen networks decrease at all  $x$  values. The swelling of hydrogels takes place in three steps: diffusion of water into the gel, relaxation of polymer chains, and then expansion of the network. According to the rubber elasticity theory, swelling is a function of the elastic nature of the polymer chains and the modulus of the gel which is directly related to the network cross-linking density.<sup>35,36</sup> The cross-linking density, the number of chemical or physical cross-links in a given volume, controls many fundamental hydrogel properties including the swelling ratio and the modulus. In summary, it is an expected result that an increase in the degree of swelling will decrease the cross-link density and thus the elastic modulus.<sup>37</sup>

Frequency sweep tests, performed within the linear viscoelastic region of each hydrogel, enabled the frequency dependence determination of the material. Figure 2A shows the

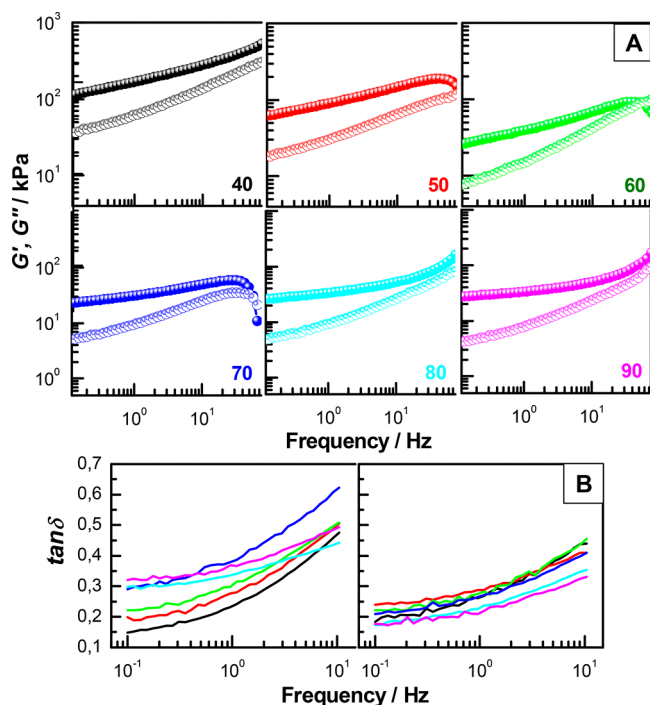


**Figure 2.** (A) Storage ( $G'$ , filled symbols) and loss modulus ( $G''$ , open symbols) of as-prepared state SM- $x$  networks as a function of frequency were measured at 37 °C. (B) Loss factor ( $\tan \delta$ ) versus frequency plot of the gels as-prepared (as, left) and swollen (sw, right) states at 37 °C.

double logarithmic plots of  $G'$  and  $G''$  versus frequency between 0.1 and 100 Hz of SM- $x$  gels after preparation at 1% strain and 37 °C. It can be seen that all of the networks exhibited a  $G'$  value that was always higher than the  $G''$  value, denoting that the elastic character is always dominant and the system in the gel state when the load is applied.<sup>38,39</sup> Both moduli increase with the increasing frequency due to the time-dependent viscoelastic character of the physical cross-links typically observed in hydrophobically modified hydrogels.<sup>40</sup> When the high frequency region of the plots belonging to the gels prepared at  $50 \leq x \leq 70$  is examined, a crossover point is seen, which is an indicator of the decrease in the elastic character of the matrix. This significantly increases the viscous modulus due to the increase in the proportion of side alkyl chains. Frequency sweep tests were also performed for the swollen state hydrogels (Figure S6).

The quantity of loss factor ( $\tan \delta$ ) represents the ratio of dissipated energy to stored energy during one deformation cycle. When the  $\tan \delta$  plots obtained from frequency sweep were examined, the value of  $\tan \delta$  was found to be greater than 0.01 over the whole frequency range in the measuring systems, which indicates the formation of the weak gels (Figure 2B).<sup>41</sup> Although a frequency-dependent behavior is observed in the SM- $x$  gels, the slope increases after a critical  $x$  value. Up to 60 mol % SM, a slightly lower slope of the  $\tan \delta$ –frequency curve was observed. With the increase of  $x \geq 60$ , as well as the increase of the slope, the value of  $\tan \delta$  was decreased. In the  $\tan \delta$  plots of the gels that reached swelling equilibrium, as the values approached each other, relatively less frequency-dependent structures were obtained.

In the case of a strain-dependent oscillatory shear test, as plotted in Figure 3, for the gels  $x < 60$ , linear viscoelasticity is

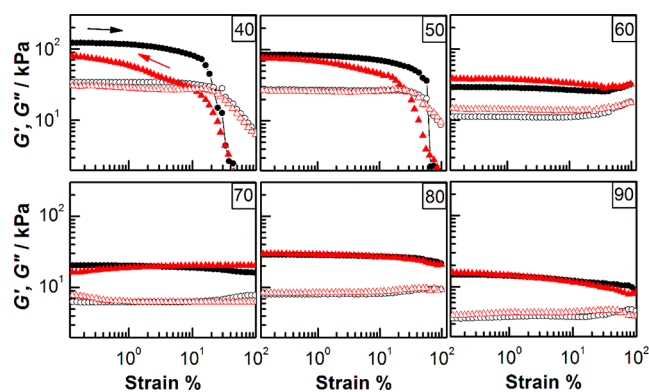


**Figure 3.** Strain sweep measurements of the as-prepared SM- $x$  networks from 0.1 to 100% (black symbols) and 100 to 0.1% (red symbols) strain with a constant frequency of 1 Hz at 37 °C.  $x$  values were indicated on the plots. Storage ( $G'$ , filled symbols) and loss modulus ( $G''$ , open symbols).

noticed initially. As the deformation in the linear viscoelastic region (LVER) is sufficiently small, the cross-linking structure of the gels remains intact, with  $G' > G''$  consistent with a solid-like material. However, after a critical strain value, an onset of nonlinearity was observed.  $G'$  decreased by about 2 orders of magnitude when  $\gamma$  increased to 100% strain, and its value crossed over with that of  $G''$  (i.e.,  $G'' > G'$ ) at higher strain values. For the gels  $x \geq 60$ , almost all of the deformation range measured constitutes the LVER that indicates the enhancement of the mechanical properties by the addition of a higher amount of hydrophobic monomer. When the return curves from 100 to 0.1% strain are examined, it is clearly seen that the gels with low SM content cannot fully return to their initial modulus values, while the gels formed with concentrations of 60% and above are completely reversible. The interactions that sustain the structure are the dipole interactions from the VP units and the hydrophobic interactions of the alkyl groups in the side chains of the SM. In these measurements made at a temperature above  $T_m$ , the crystalline alkyl chains are in a molten state. It can be seen from the deformation sweep that SM interactions in the dynamic structure are quite effective in the self-healing of the material after deformation compared to VP.

Strain sweep measurements were also performed in the swollen state (Figure S6). In Figure 4, strain sweep measurements of as-prepared and swollen gels are given comparatively. It is clearly shown that, regardless of the concentration, the LVER of the networks becomes smaller by swelling. The narrowing of the LVER with swelling will lead to a decrease in the mechanical strength of the gels.

Mechanical properties of the networks were analyzed by using uniaxial compression and elongation tests. Parts A and B of Figure 4 demonstrate the digital photograph of a cylindrical-shaped SM-40 gel during the compression test and the stress–strain plot of the measurement at 37 °C, respectively. In a typical plot of the gels with dynamic cross-linking structure, the nominal stress  $\sigma_{nom}$  increases continuously with increasing deformation even though the gels are almost completely compressed. Therefore, to determine the fracture stress ( $\sigma_f$ ) and deformation ( $\lambda_f$ ) values, the stress was presented by its  $\sigma_{nom}$  or true stress values  $\sigma_{true} (= \lambda \sigma_{nom})$ , which are the forces per cross-sectional

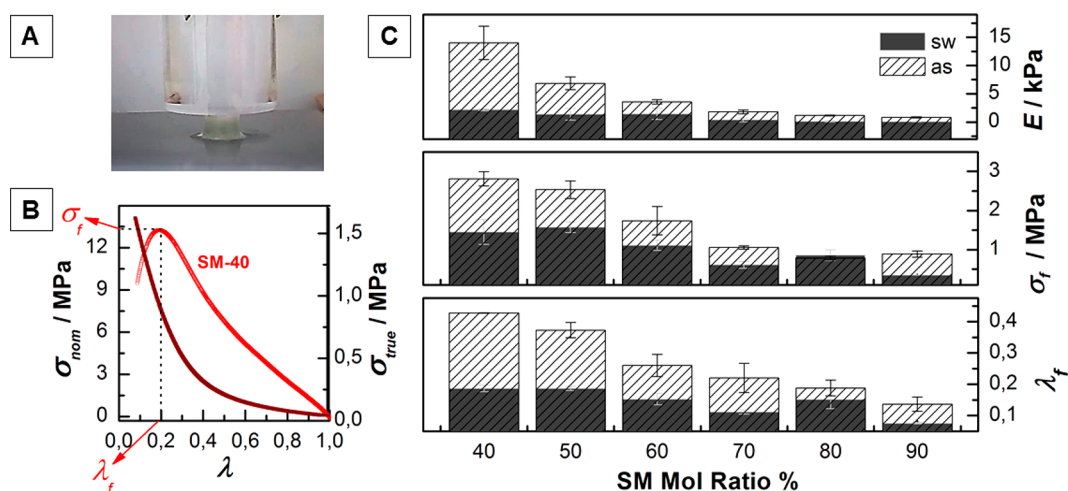


**Figure 4.** Compression tests of SM- $x$  networks as-prepared and swollen states at 37 °C. (A) Photograph of a SM-40 hydrogel during the compression test and (B) a typical stress–strain curve of the measurement. (C) Young's moduli  $E$ , fracture stress  $\sigma_f$ , and fracture deformation  $\lambda_f$  plotted against SM mol ratio %.

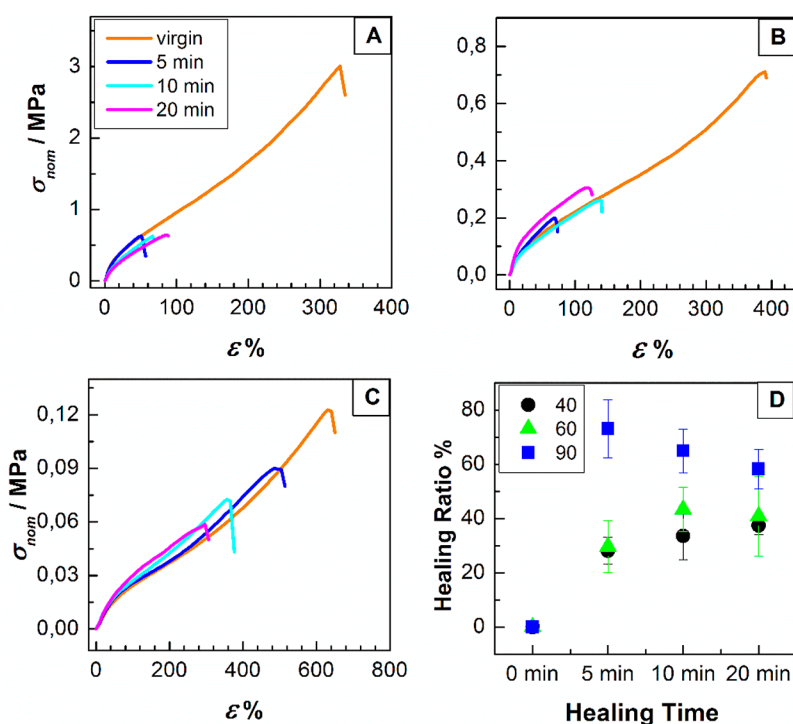


**Figure 5.** (A–C) Tensile stress–strain plots of the virgin and healed SM- $x$  networks performed at varying healing times. (A) SM-40, (B) SM-60, and (C) SM-90. (D) Healing ratio–healing time plot of the SM- $x$  networks.

area of the undeformed and deformed gel specimen (Figure 4B).<sup>10</sup> According to Figure 4C, the initial slope of the curves, that is, the compressive Young's modulus  $E$ ,  $\sigma_f$ , and  $\lambda_f$ , decreases as a function of SM mol ratio, indicating that the mechanical property is controllable by the amount of SM introduced into the reaction medium. As an example,  $E$  decreases from 16 to 1 kPa as the SM ratio increases to 90 mol %. Similar to the results of the rheological analysis, performing the measurements above  $T_m$  leads to the melting of the crystal regions, revealing the effect of VP units in the network more. Compression tests were also applied to the samples that reached swelling equilibrium. The fact that the gels become less frequency-dependent after swelling and have a narrower LVR also causes a decrease in their mechanical strength (Figures 2 and 4). As with the rheological

measurements, the compressive Young's modulus decreased compared to the post-synthesis gels. Similarly, the maximum force that must be applied to disrupt the structural integrity of the gels,  $\sigma_f$  and the maximum deformation values that the gels can withstand,  $\lambda_f$ , decreased with swelling. It has been witnessed in the compression measurements how the frequency and strain sweep outputs determine the properties of the macrostructure.

As a result of uniaxial tensile tests performed at different concentrations, it was observed that the tensile strength and toughness increased with increasing value of  $x$ . According to the measurement, the elongation at break of  $318 \pm 14$  value obtained for SM-40 increased to  $633 \pm 29$  for SM-90. In order to follow the self-healing properties of the gels, the razor-cut gel tips were brought together and subjected to the tensile measure-

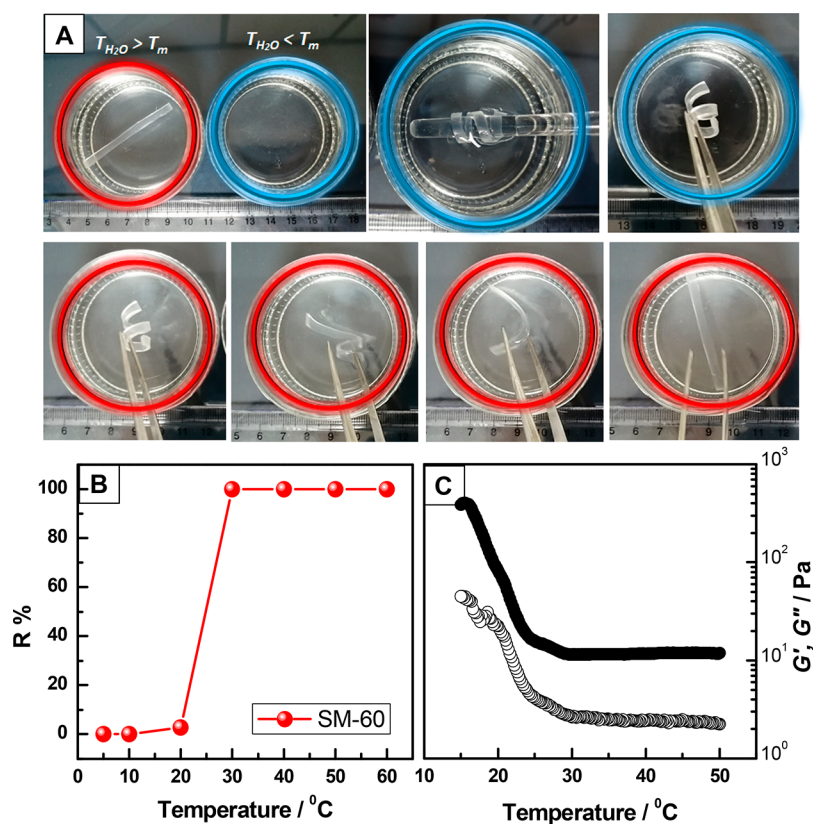


**Figure 6.** (A) Images demonstrating the shape memory behavior of the swollen state SM-90 network. (B) Shape recovery ratio, R%, as a function of temperature. (C) Temperature dependency of  $G'$  (filled symbols) and  $G''$  (open symbols) for the swollen state SM-60 network.

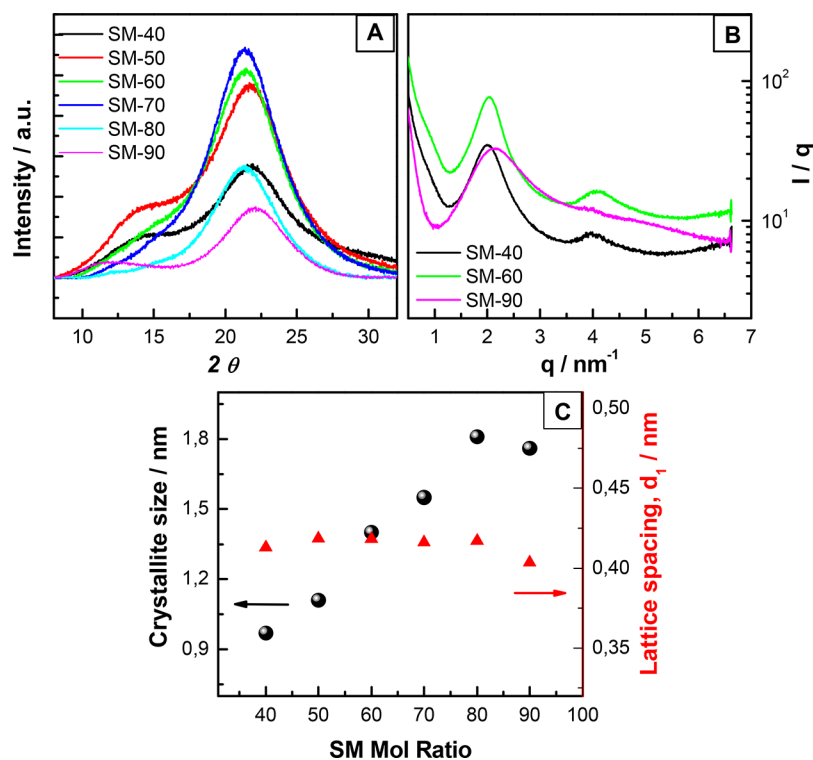


**Figure 7.** (A) XRD patterns of swollen state SM-*x* networks in the 5–35  $^{\circ}$   $2\theta$  range with a scan rate of 1  $^{\circ}/\text{min}$ . (B) WAXS patterns of swollen state SM-*x* networks measured at room temperature. (C) Crystallite size and lattice spacing calculated from the XRD plot.

ments at the end of changing healing times. Healing processes were performed at the body temperature which is above the  $T_m$

value. As given in Figure 5, it was observed that the recovery efficiencies increased with increasing ratio of SM. The most

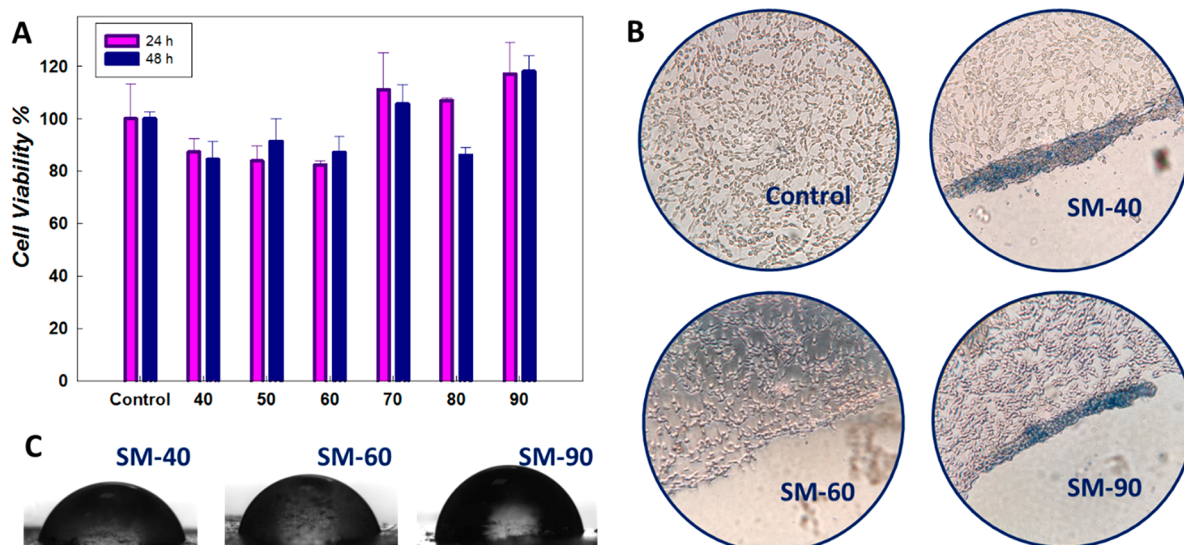


**Figure 8.** Cytotoxicity of SM- $x$  hydrogels against human skin fibroblast cells evaluated after direct contact test by MTT assay. (A) Cell viability (%) values of CDD cells contacted with gels at 24 and 48 h. (B) Representative trypan blue dye images of CCD cells after removal of the SM gels. (C) Water contact angle (WCA) measurements.

striking point in the self-healing tests is that, when the healing time increases, the healing rate increases proportionally in the SM-40 and SM-60 gels, while the opposite behavior is observed in the gels with the highest SM ratio. It is thought that the decrease in healing efficiencies due to the increased healing time in SM-90 gels is possibly related to the temperature at which the tests are performed. While the cutoff gels are kept at 37 °C, the measurements are taken at room temperature. No matter how fast the gels are treated, some cooling of the gels reduces the healing efficiency of SM-90 gels with a  $T_m$  value of around 30 °C. Since SM-90 gels, whose ends stick together when cut with a razor blade, harden when cooled, their elongation values are lower than they should be.

A swollen SM-60 gel was used to demonstrate the shape memory feature, which is another property of the semicrystalline SM- $x$  network structures. The gel sample in the form of a flat rod was spiraled above the  $T_m$  value, and this shape was fixed at a temperature below  $T_m$ . Later, when the gel sample was immersed in hot water again, it was observed that it reached the permanent rod form in a very short time (Figure 6). In order to quantitatively examine the shape memory feature depending on the SM ratio, a bending test at various temperatures was applied to the swollen state networks. Shape recovery ratios, R%, of the SM-60 networks are plotted against the temperature in Figure 6B. The recovery ratio gradually increased with increasing temperature due to the simultaneous melting of the crystalline side chains in the network. It was observed that the SM-60 gel started to change its temporary shape into its permanent one at 20 °C with a value of R% = 3. The recovery ratio was increased rapidly with the increasing temperature and reached up to 100% above 30 °C. This behavior proportional to the melting of the side alkyl chains is also supported by the temperature profile given in Figure 6C. Consistent with the shape memory test, the network transition was observed as the  $G'$  and  $G''$  were decreased with increasing temperature between 15 and 30 °C. In addition to the fact that the gels can completely return to their permanent form, the recovery processes take less than 6 s for SM-40 and SM-60 (Figure S7). Shape memory properties of SM-90 gels could not be determined quantitatively due to the sticking (self-healing) of the folded gel structures to

each other during the bending test. It has been observed that the gels regained their permanent state when both of the gel tips were not completely superposed on each other.

The microstructures of the gels were analyzed by XRD and WAXS. Figure 7 shows the XRD pattern of the swollen SM- $x$  networks with varying  $x$  values. All of the gel samples show a peak at around  $2\theta = 21^\circ$ , corresponding to a Bragg  $d$ -spacing of  $0.41 \pm 0.06$  nm between the long alkyl chains of stearyl methacrylates. This value is in agreement with the value of several long chain alkyl crystals.<sup>42–44</sup> Apparent crystalline dimensions along the lattice direction were also calculated by measuring the half-width at midheight of the corresponding Bragg reflection and by applying the Scherrer formula.<sup>45</sup> As given in Figure 7C, the crystallite sizes increase in proportion to the increasing amount of SM up to a ratio of 90. A larger fraction of the amorphous component VP in the matrix acts as a steric barrier and limits the growth of alkyl crystals that prevents the formation of large polymer crystals.<sup>46</sup> Figure 7B shows the WAXS patterns of swollen state networks of SM-40, SM-60, and SM-90. All gels exhibited a broad diffraction peak in the low  $q$  region ( $q = 1.9 \text{ nm}^{-1}$ ) attributed to the diffraction of alkyl nanodomains, while SM-40 and SM-60 showed a small peak at  $q = 4.0 \text{ nm}^{-1}$  due to partially crystallized side chain domains.<sup>47</sup>

To examine the biocompatibility of the SM- $x$  networks, the cytotoxicity was assessed *in vitro* by a colorimetric MTT test. The cytotoxicity against human skin fibroblast cells CCD-986Sk was determined as a function of the SM concentration (Figure 8). Cells cultured in the presence of the gel samples were tested by the addition of MTT reagent after the removal of the gel samples. SM- $x$  hydrogels do not show significant cytotoxicity. The viability of the incubated cells was over 82% in all  $x$  values, and the increase in cell viabilities at high SM ratios is remarkable. More than 100% cell viability was obtained at  $x$  values above 60. As shown in Figure 8C, SM- $x$  networks gain more hydrophobic characteristics by increasing SM ratio, such as the water contact angles (WCAs) that were measured as 54° for SM-40 and increased up to 78° for SM-90. In more hydrophobic gel systems ( $x > 60$ ), cells prefer to spread around the gel, rather than proliferating on the gel surface, as it is much more difficult for cells to adhere to hydrophobic surfaces.<sup>48</sup> Therefore, higher cell

viability results were obtained from more hydrophobic gel samples ( $x > 60$ ) than less hydrophobic ones, as some of the cells were lost before the MTT reagent addition by the removal of gel samples with the adhered cells on its surface. These discarded gel sample surfaces, so adhesion of cells on them, have been followed by microscopy. In gels with  $x \leq 60$ , on the other hand, relatively lower cell viability values were obtained, as the cells could also proliferate through the gel surface. Higher magnification images of CCD cells stained with Hoechst and propidium iodide (PI) dye grown on the SM-60 gel network were added in Figure S9 to observe the cell morphology clearly.

Cell adhesion onto SM- $x$  gels was evidenced through the fluorescence microscopy images by staining with Hoechst dye. It was observed from Figure S10 that CCD cells could adhere to SM-60 networks and both the adhesion and attachment of the cells increased with time (after 48 h). It was observed that the cells could spread toward the middle of the gel sample in 48 h of incubation, while in 24 h they were merely able to be reached to localize at the edges of the gel samples. Even though the wells were washed with PBS after staining, there was an excess of background fluorescence in the photographs, which may have originated from a variety of sources. Instead of special imaging dishes like glass-bottom dishes, typical plastic-bottom cell culture plates were used that can fluoresce and cause a high background. Second, the hydrogels themselves may also have caused the fluorescence background.

It is known with the metal or metal-alloy implants that, even though they compensate the required biomechanical properties, the tissue-material integration may fail due to the lack of interfacial bonding for orthopedic implants.<sup>49</sup> Direct integration of material to living bone called “osseointegration” is also reported as a vital key point as well as the epithelial cell attachment for the success of dental implant.<sup>50</sup> On the other hand, for blood contacting materials, it is an issue of hemocompatibility which is investigated by the researchers in a wide variety by designing passivated, functionalized, and a combination of both surfaces.<sup>51</sup> In light of these, the wide range of properties of SM- $x$  gel samples, in physicochemical, mechanical, and biological aspects, may show a significant potential to address various needs within several biomedical applications.

#### 4. CONCLUSIONS

In this study, SM- $x$  networks were formed only in the presence of crystalline structures and/or hydrophobic interactions and dipole–dipole interactions by combining hydrophobic SM units with long alkyl side chains and hydrophilic monomer VP. SM mol ratios were gradually changed between 10 and 90% to examine the effect of hydrophobic and hydrophilic components on the properties of the final gels. Melting peak enthalpies of the DSC thermograms were used to calculate the degree of crystallinity,  $f$  %, originated from the side alkyl chains of SM, increasing parallel to the amount of SM. In addition to the DSC analysis, the decrease in swelling values with increasing  $x$  indicated that long alkyl chains were effectively incorporated into the structure as cross-linkers. The storage modulus,  $G'$ , which is measured above the  $T_m$  value, decreases rapidly due to increased SM concentrations up to a mol ratio of 60% but does not change much after this concentration. When the alkyl crystals are in the molten state, the presence of VP structures becomes more dominant over the modulus values due to dipole forces. All of the SM- $x$  networks show a time-dependent viscoelastic character typically observed in hydrophobically

modified hydrogels. Low SM content gels cannot fully return to their initial modulus values, while the gels formed with concentrations of 60% and above are completely reversible due to the dynamic hydrophobic interactions which are also effective in the self-healing of the material. Uniaxial compression and tensile tests show that the mechanical properties are controllable by the amount of SM introduced into the reaction medium. All of the networks can completely return to their permanent form in seconds. The crystallite sizes determined by XRD analysis increase in proportion to the increasing amount of SM up to the ratio of 90. The cytotoxicity of the networks assessed against human skin fibroblast cells CCD-986Sk was determined. While the viability of cells closely related with the water contact angle of the networks measured as  $54^\circ$  for SM-40 increased to  $78^\circ$  for SM-90, it remained above 82% at all  $x$  values, meaning that the SM- $x$  hydrogels do not show significant cytotoxicity and are suitable for the possible bio applications.

#### ■ ASSOCIATED CONTENT

##### Supporting Information

The Supporting Information is available free of charge at <https://pubs.acs.org/doi/10.1021/acsapm.1c01565>.

Obtained parameters from DSC and compression analysis (PDF)

#### ■ AUTHOR INFORMATION

##### Corresponding Author

Deniz Ceylan Tuncaboğlu – *Bezmiâlem Vakıf University, Faculty of Pharmacy, 34093 Istanbul, Turkey*; [orcid.org/0000-0001-6853-3493](https://orcid.org/0000-0001-6853-3493); Email: [dtuncaboğlu@bezmi alem.edu.tr](mailto:dtuncaboğlu@bezmi alem.edu.tr)

##### Authors

Hüsna Kılıç – *Bezmiâlem Vakıf University, Health Sciences Institute, Department of Biotechnology, 34093 Istanbul, Turkey*

Aslıhan Argun – *Le Mans University, Institute of Molecules and Materials (IMMM), 72085 Cedex 9 Le Mans, France; Regenerative Medicine and Skeleton Dental Faculty-1 INSERM UMR 1229, 44042 Nantes, France; Istanbul Technical University, Department of Chemistry, 34469 Istanbul, Turkey*

Dilek Öztürk Civelek – *Bezmiâlem Vakıf University, Faculty of Pharmacy, 34093 Istanbul, Turkey*

Complete contact information is available at: <https://pubs.acs.org/doi/10.1021/acsapm.1c01565>

##### Notes

The authors declare no competing financial interest.

#### ■ ACKNOWLEDGMENTS

This study was financially supported by the Scientific Research Projects Committee of Bezmiâlem Vakıf University (BAP, 12.2018/19), Istanbul, Turkey. We thank Çiğdem Bilici for the XRD measurements.

#### ■ REFERENCES

- (1) Hao, J.; Weiss, R. A. Viscoelastic and Mechanical Behavior of Hydrophobically Modified Hydrogels. *Macromolecules* **2011**, *44* (23), 9390–9398.

- (2) Rao, Z.; Inoue, M.; Matsuda, M.; Taguchi, T. Quick self-healing and thermo-reversible liposome gel. *Colloids Surf., B* **2011**, *82* (1), 196–202.
- (3) Tuncaboylu, D. C.; Sari, M.; Oppermann, W.; Okay, O. Tough and Self-Healing Hydrogels Formed via Hydrophobic Interactions. *Macromolecules* **2011**, *44* (12), 4997–5005.
- (4) Tuncaboylu, D. C.; Argun, A.; Sahin, M.; Sari, M.; Okay, O. Structure optimization of self-healing hydrogels formed via hydrophobic interactions. *Polymer* **2012**, *53* (24), 5513–5522.
- (5) Tuncaboylu, D. C.; Sahin, M.; Argun, A.; Oppermann, W.; Okay, O. Dynamics and Large Strain Behavior of Self-Healing Hydrogels with and without Surfactants. *Macromolecules* **2012**, *45* (4), 1991–2000.
- (6) Akay, G.; Hassan-Raeisi, A.; Tuncaboylu, D. C.; Orakdogan, N.; Abdurrahmanoglu, S.; Oppermann, W.; Okay, O. Self-healing hydrogels formed in cationic surfactant solutions. *Soft Matter* **2013**, *9* (7), 2254–2261.
- (7) Gulyuz, U.; Okay, O. Self-healing polyacrylic acid hydrogels. *Soft Matter* **2013**, *9* (43), 10287–10293.
- (8) Hao, X.; Liu, H.; Lu, Z.; Xie, Y.; Yang, H. Endowing the conventional HMPAM hydrogel with pH-responsive and self-healing properties. *Journal of Materials Chemistry A* **2013**, *1* (23), 6920–6927.
- (9) Tuncaboylu, D. C.; Argun, A.; Algi, M. P.; Okay, O. Autonomic self-healing in covalently crosslinked hydrogels containing hydrophobic domains. *Polymer* **2013**, *54* (23), 6381–6388.
- (10) Argun, A.; Algi, M. P.; Tuncaboylu, D. C.; Okay, O. Surfactant-induced healing of tough hydrogels formed via hydrophobic interactions. *Colloid Polym. Sci.* **2014**, *292* (2), 511–517.
- (11) Deng, G.; Tang, C.; Li, F.; Jiang, H.; Chen, Y. Covalent Cross-Linked Polymer Gels with Reversible Sol–Gel Transition and Self-Healing Properties. *Macromolecules* **2010**, *43* (3), 1191–1194.
- (12) Liu, F.; Li, F.; Deng, G.; Chen, Y.; Zhang, B.; Zhang, J.; Liu, C.-Y. Rheological Images of Dynamic Covalent Polymer Networks and Mechanisms behind Mechanical and Self-Healing Properties. *Macromolecules* **2012**, *45* (3), 1636–1645.
- (13) Zhang, Y.; Tao, L.; Li, S.; Wei, Y. Synthesis of Multiresponsive and Dynamic Chitosan-Based Hydrogels for Controlled Release of Bioactive Molecules. *Biomacromolecules* **2011**, *12* (8), 2894–2901.
- (14) He, L.; Fullenkamp, D. E.; Rivera, J. G.; Messersmith, P. B. pH responsive self-healing hydrogels formed by boronate-catechol complexation. *Chem. Commun.* **2011**, *47* (26), 7497–7499.
- (15) Shafiq, Z.; Cui, J.; Pastor-Pérez, L.; San Miguel, V.; Gropeanu, R. A.; Serrano, C.; del Campo, A. Bioinspired Underwater Bonding and Debonding on Demand. *Angew. Chem.* **2012**, *124* (18), 4408–4411.
- (16) Wong Po Foo, C. T. S.; Lee, J. S.; Mulyasmita, W.; Parisi-Amon, A.; Heilshorn, S. C. Two-component protein-engineered physical hydrogels for cell encapsulation. *Proc. Natl. Acad. Sci. U. S. A.* **2009**, *106* (52), 22067–22072.
- (17) Appel, E. A.; Biedermann, F.; Rauwald, U.; Jones, S. T.; Zayed, J. M.; Scherman, O. A. Supramolecular Cross-Linked Networks via Host–Guest Complexation with Cucurbit[8]uril. *J. Am. Chem. Soc.* **2010**, *132* (40), 14251–14260.
- (18) Skrzyszewska, P. J.; Sprakel, J.; de Wolf, F. A.; Fokkink, R.; Cohen Stuart, M. A.; van der Gucht, J. Fracture and Self-Healing in a Well-Defined Self-Assembled Polymer Network. *Macromolecules* **2010**, *43* (7), 3542–3548.
- (19) Behl, M.; Razaq, M. Y.; Lendlein, A. Multifunctional Shape-Memory Polymers. *Adv. Mater.* **2010**, *22* (31), 3388–3410.
- (20) Xu, S.; Zhao, B.; Raza, M.; Li, L.; Wang, H.; Zheng, S. Shape Memory and Self-Healing Nanocomposites with POSS–POSS Interactions and Quadruple Hydrogen Bonds. *ACS Applied Polymer Materials* **2020**, *2* (8), 3327–3338.
- (21) Qiao, L.; Liu, C.; Liu, C.; Zong, L.; Gu, H.; Wang, C.; Jian, X. Self-healing, pH-sensitive and shape memory hydrogels based on acylhydrazone and hydrogen bonds. *Eur. Polym. J.* **2022**, *162*, 110838.
- (22) Kurt, B.; Gulyuz, U.; Demir, D. D.; Okay, O. High-strength semi-crystalline hydrogels with self-healing and shape memory functions. *Eur. Polym. J.* **2016**, *81*, 12–23.
- (23) Argun, A.; Gulyuz, U.; Okay, O. Semi-Crystalline, Three-Segmented Hybrid Gels with Multiple Shape-Memory Effect. *Macromol. Symp.* **2019**, *385* (1), 1800164.
- (24) Argun, A.; Gulyuz, U.; Okay, O. Interfacing Soft and Hard Materials with Triple-Shape-Memory and Self-Healing Functions. *Macromolecules* **2018**, *51* (7), 2437–2446.
- (25) Mogri, Z.; Paul, D. R. Gas sorption and transport in side-chain crystalline and molten poly(octadecyl acrylate). *Polymer* **2001**, *42* (6), 2531–2542.
- (26) Bisht, H.; Pande, P.; Chatterjee, A. Docosyl acrylate modified polyacrylic acid: Synthesis and crystallinity. *European Polymer Journal - EUR POLYM J.* **2002**, *38*, 2355–2358.
- (27) Bilici, C.; Can, V.; Nöchel, U.; Behl, M.; Lendlein, A.; Okay, O. Melt-Processable Shape-Memory Hydrogels with Self-Healing Ability of High Mechanical Strength. *Macromolecules* **2016**, *49* (19), 7442–7449.
- (28) Behl, M.; Zhao, Q.; Lendlein, A. Glucose-responsive shape-memory cryogels. *J. Mater. Res.* **2020**, *35* (18), 2396–2404.
- (29) ISO 10993-5:2009. Biological Evaluation of Medical Devices. *Tests for in Vitro Cytotoxicity*; 2009.
- (30) Franco, R. A.; Min, Y. K.; Yang, H. M.; Lee, B. T. Fabrication and biocompatibility of novel bilayer scaffold for skin tissue engineering applications. *J. Biomater. Appl.* **2013**, *27* (5), 605–15.
- (31) Habibi, A.; Vasheghani-Farahani, E.; Semsarzadeh, M.; Sadaghiani, K. Monomer reactivity ratios for lauryl methacrylate–isobutyl methacrylate in bulk free radical copolymerization. *Polym. Int.* **2003**, *52* (9), 1434–1443.
- (32) Mitsoni, E.; Roka, N.; Pitsikalis, M. Statistical copolymerization of N-vinyl-pyrrolidone and alkyl methacrylates via RAFT: reactivity ratios and thermal analysis. *Journal of Polymer Research* **2019**, *26* (5), 118.
- (33) Faragalla, M.; Hill, D.; Whittaker, A. The copolymerization of N-vinyl-2-pyrrolidone with 2-hydroxyethyl methacrylate. *Polym. Bull.* **2002**, *47*, 421–427.
- (34) Park, W. H.; Kim, M. Chemically cross-linked silk fibroin hydrogel with enhanced elastic properties, Biodegradability, and biocompatibility. *Int. J. Nanomed.* **2016**, *11*, 2967.
- (35) Flory, P. J.; Rehner, J. Statistical Mechanics of Cross-Linked Polymer Networks II. Swelling. *J. Chem. Phys.* **1943**, *11* (11), 521–526.
- (36) Flory, P. J.; Rehner, J. Statistical Mechanics of Cross-Linked Polymer Networks I. Rubberlike Elasticity. *J. Chem. Phys.* **1943**, *11* (11), 512–520.
- (37) Yin, H.; Akasaki, T.; Sun, T.; Nakajima, T.; Kurokawa, T.; Nonoyama, T.; Taira, T.; Saruwatari, Y.; Gong, J. Double network hydrogels from polyzwitterions: High mechanical strength and excellent anti-biofouling properties. *J. Mater. Chem. B* **2013**, *1*, 3685.
- (38) Cuomo, F.; Cofelice, M.; Lopez, F. Rheological Characterization of Hydrogels from Alginate-Based Nanodispersion. *Polymers* **2019**, *11* (2), 259.
- (39) Jaishankar, A.; McKinley, G. Power-law rheology in the bulk and at the interface: Quasi-properties and fractional constitutive equations. *Proceedings of the Royal Society A: Mathematical, Physical and Engineering Science* **2013**, *469*, 20120284.
- (40) Abdurrahmanoglu, S.; Can, V.; Okay, O. Design of high-toughness polyacrylamide hydrogels by hydrophobic modification. *Polymer* **2009**, *50* (23), 5449–5455.
- (41) Ross-Murphy, S. B.; Morris, V. J.; Morris, E. R. Molecular viscoelasticity of xanthan polysaccharide. *Faraday Symp. Chem. Soc.* **1983**, *18* (0), 115–129.
- (42) Matsuda, A.; Sato, J. i.; Yasunaga, H.; Osada, Y. Order-Disorder Transition of a Hydrogel Containing an n-Alkyl Acrylate. *Macromolecules* **1994**, *27* (26), 7695–7698.
- (43) Platé, N. A.; Shibaev, V. P.; Petrukhin, B. S.; Zubov, Y. A.; Kargin, V. A. Structure of crystalline polymers with unbranched long side chains. *Journal of Polymer Science Part A-1: Polymer Chemistry* **1971**, *9* (8), 2291–2298.
- (44) Bilici, C.; Ide, S.; Okay, O. Yielding Behavior of Tough Semicrystalline Hydrogels. *Macromolecules* **2017**, *50* (9), 3647–3654.

(45) Jagodzinski, H.; Klug, H. P.; Alexander, L. E. X-ray Diffraction Procedures for Polycrystalline and Amorphous Materials, 2. Auflage. John Wiley & Sons, New York-Sydney-Toronto 1974, 966 Seiten, Preis: £ 18.55. *Berichte der Bunsengesellschaft für physikalische Chemie* **1975**, *79* (6), 553–553.

(46) Ricciardi, R.; De Rosa, C.; Lauprêtre, F. X-ray Diffraction Analysis of Poly(vinyl alcohol) Hydrogels, Obtained by Freezing and Thawing Techniques. *Macromolecules* **2004**, *37*, 1921.

(47) Ebata, K.; Hashimoto, Y.; Yamamoto, S.; Mitsuishi, M.; Nagano, S.; Matsui, J. Nanophase Separation of Poly(N-alkyl acrylamides): The Dependence of the Formation of Lamellar Structures on Their Alkyl Side Chains. *Macromolecules* **2019**, *52* (24), 9773–9780.

(48) Ahmed, M.; Ramos, T. A. d. S.; Damanik, F.; Quang Le, B.; Wieringa, P.; Bennink, M.; van Blitterswijk, C.; de Boer, J.; Moroni, L. A combinatorial approach towards the design of nanofibrous scaffolds for chondrogenesis. *Sci. Rep.* **2015**, *5* (1), 14804.

(49) Chen, J. Thin film coatings and the biological interface. In *Thin Film Coatings for Biomaterials and Biomedical Applications*; Griesser, H. J., Ed.; Woodhead Publishing: 2016; pp 143–164.

(50) Guo, C. Y.; Matinlinna, J. P.; Tang, A. T. H. Effects of Surface Charges on Dental Implants: Past, Present, and Future. *International Journal of Biomaterials* **2012**, *2012*, 381535.

(51) Qiao, Y.; Liu, X. Biocompatible Coating. In *Comprehensive Materials Processing*; Hashmi, S., Batalha, G. F., Van Tyne, C. J., Yilbas, B., Eds.; Elsevier: Oxford, U.K., 2014; pp 425–447.

## Recommended by ACS

### Low-Friction Hybrid Hydrogel with Excellent Mechanical Properties for Simulating Articular Cartilage Movement

Zhongnan Wang, Hui Guo, *et al.*

FEBRUARY 01, 2023

LANGMUIR

READ 

### Strong Biopolymer-Based Nanocomposite Hydrogel Adhesives with Removability and Reusability for Damaged Tissue Closure and Healing

Yu Tian, Lei Zhou, *et al.*

DECEMBER 03, 2022

ACS APPLIED MATERIALS & INTERFACES

READ 

### Photoacidity and Photodegradation within Polyelectrolyte/TiO<sub>2</sub> Suspensions and Coatings

Martin Müller, Andreas Fery, *et al.*

NOVEMBER 15, 2022

ACS APPLIED POLYMER MATERIALS

READ 

### Structure, Morphology, and Surface Chemistry of Surgical Masks and Their Evolution up to 10 Washing Cycles

Louise Wittmann, José Penuelas, *et al.*

FEBRUARY 23, 2023

ACS APPLIED POLYMER MATERIALS

READ 

Get More Suggestions >